RESEARCH ARTICLE

Investigating the Effect of Center of Rotation of Angulation (CORA) Location on Varus Knee Joint Mechanics

Reyhaneh Rostamian, PhD; Masoud Shariat Panahi, PhD; Morad Karimpour, PhD; Mahdie Aghasizade, PhD; Hadi G. Kashani, PhD

Research performed at University of Tehran, Tehran, Iran

Received: 22 February 2025 *Accepted: 19 August 2025*

Abstract

Objectives: Malalignment of the lower limb, such as varus deformity, can impair function by altering joint biomechanics and gait. However, the effect of the center of rotation of angulation (CORA) location on joint mechanics in varus deformity remains unclear.

Methods: This study proposed an approach to enhance the accuracy and efficiency of joint kinetics and kinematics estimation during gait by incorporating precise CORA positioning along the femur. Simulations were performed using inverse kinematics and dynamics for a 10° varus deformity. The deformities were modeled with CORA located at fractions ranging from 1/6 to 5/6 of femoral length (measured from the hip to the knee joint), and were compared with a baseline representing normal lower-limb alignment.

Results: The findings indicated that varus deformity had a minimal effect on the subtalar angle but substantially altered the subtalar moment during stance. CORA placement near the hip joint increased both ankle plantar-/dorsiflexion and knee flexion/extension angles. Proximal CORA positioning also influenced joint reaction forces, producing higher forces at the ankle and reduced forces at the hip. While hip abduction/adduction moments showed only minor changes, hip rotation moments varied considerably across CORA locations, particularly during stance.

Conclusion: Incorporating CORA into deformity modeling enables more accurate simulation of pathological alignment, providing detailed insights into joint kinetics and kinematics. Such information can help surgeons better understand patient-specific conditions and develop more precise surgical plans.

Level of evidence: V

Keywords: Gait analysis, Lower limb skeletal disorders, The location of the center of rotation of angulation, Varus deformity

Introduction

Pathological genu varus is defined as a condition in which the mechanical axis angle of the lower limb exceeds 1.3°. The mechanical axis angle is measured as the angle between a line drawn from the femoral head center to the intercondylar notch center of the femur and a line drawn from the talar center of the ankle to the midpoint of the tibial spine tips.[1] Genu varus may result from deformities of the femur, tibia, or joint line, which can be identified by measuring the mechanical lateral distal femoral angle (MLDFA), the mechanical medial proximal tibial angle (MMPTA), and the joint line convergence angle (JLCA).[2,3] This malalignment increases loading on the medial compartment of the knee during gait and may lead to progressive structural damage, such as knee osteoarthritis, affecting more than 12% of adults.[4,5] Consequently, orthopedic surgeons are particularly interested in evaluating the kinematics and kinetics of lower-extremity joints during locomotion.[6,7] However, static imaging techniques, such as computed tomography (CT), are insufficient for assessing varus deformities, as

Corresponding Author: Reyhaneh Rostamian, School of Mechanical Engineering, University of Tehran, Tehran, Iran

Email: Reyhaneh.rostamian@gmail.com

THE ONLINE VERSION OF THIS ARTICLE ABJS.MUMS.AC.IR

they fail to account for primary and secondary gait deviations.[2] Therefore, three-dimensional gait analysis is recommended for preoperative planning to accurately characterize and manage these abnormalities.[8]

Previous studies have demonstrated that varus deformity can lead to abnormal gait patterns.[9,10] The literature indicates that even a 10° varus deformity can substantially increase peak contact forces during walking.[2] In addition, secondary gait deviations—including medial weight shift at the foot, ipsilateral trunk lean, and toe-out—have been observed in patients with varus deformities.[11] To address these issues, recent studies have incorporated patient-specific musculoskeletal models to account for bone deformities.[12,13] Although these models provide accurate estimations of joint forces, they are often time-consuming and costly. Alternatively, semi-personalized approaches have been proposed, in which generic models are adapted to replicate the patient's deformity.[14] However, it remains unclear how variations in the anatomical origin of varus deformity influence joint biomechanics.

This study aimed to develop a method for improving the accuracy of joint kinetics and kinematics estimation during gait in adolescents with varus deformity by precisely identifying the center of rotation of angulation (CORA). The CORA defines the origin of the deformity and represents the center of the excessive hinge in the bone, which can lead to malalignment of the mechanical or anatomical axes. To restore normal bone anatomy, performing an osteotomy at the CORA location is considered the optimal choice, as it ensures proper alignment and minimizes bony mismatch; in contrast, selecting a different origin may create an additional hinge.[15] Precise CORA positioning also influences muscle paths and force directions. In this study, we investigated how variations in CORA location affect the kinematics and moments of the pelvis, hip, knee, and ankle joints. Specifically, gait kinematics and dynamics were analyzed in a patient with a 10° varus deformity. The deformity was modeled with CORA positions ranging from 1/6 to 5/6 of femoral length, measured from the hip to the knee joint. For comparison, a normally aligned lower limb musculoskeletal model (without deformity) was also analyzed. Joint angles and moments were estimated using inverse kinematics and inverse dynamics, respectively. Muscle activations and joint reaction forces (JRFs) were determined through static optimization and the Analyze tool in OpenSim. An open-source varus–valgus tool, an open-source musculoskeletal model, and the OpenSim software platform were employed to conduct the simulations.[14,16]

Materials and Methods

Musculoskeletal Models

To construct the neuromusculoskeletal model, we employed the OpenSim 2392 full-body musculoskeletal model.[16] This model comprises 92 muscle–tendon actuators, representing 76 muscles of the lower limbs and torso. It features 23 degrees of freedom (DOF), including: 3 DOF at each hip joint (flexion/extension, internal/external rotation, and abduction/adduction); 1 DOF at each knee joint (flexion/extension); 1 DOF at each ankle joint (plantarflexion/dorsiflexion); 1 DOF at the metatarsophalangeal joint; 1 DOF at the subtalar joint (inversion/eversion); 6 DOF at the ground–pelvis joint (3 translational and three rotational); and three rotational DOF between the pelvis and torso.[17]

In this study, we employed the OpenSim 2392 gait dataset for musculoskeletal modeling. This model was chosen because it provides a well-established benchmark representing a healthy individual. The dataset included complete motion data from a 31-year-old male subject (72.6 kg, 180 cm), along with scaling factors, motion-capture trajectories, and ground reaction forces recorded during walking.

Variations of deformities

The 2392 musculoskeletal model was modified to simulate varus deformity at different origins along the femur **[Figure 1].** Six deformed models were generated from the baseline (normal) model, each with a distinct CORA. All deformed models incorporated a 10° femoral varus deformity, with CORA positions ranging from 1/6 to 5/6 of the total femoral length (i.e., 1/6, 2/6, 3/6, 4/6, and 5/6). To ensure consistency, all CORA ratios were defined relative to the distal joint (knee).

We developed a semi-personalized musculoskeletal model that incorporated patient-specific anthropometric data, including height, weight, body segment parameters, and femoral varus abnormalities, such as deformity magnitude (based on MLDFA) and deformity origin (based on CORA positioning). To introduce femoral varus deformity, we used a varus–valgus tool.[14] In its original version, the user was required to manually define the CORA to generate the deformity. We modified the tool to improve both convenience and accuracy in determining CORA location. Specifically, we defined CORA positioning as the ratio of the distance from the CORA to the distal joint relative to the total length of the femur. For femoral deformity modeling, the foot, ankle joint, tibia, fibula, and knee joint were rotated by the full deformity angle (MLDFA) in the coronal plane. Subsequently, the femur was deformed according to the defined CORA, and the corresponding muscle attachments were adjusted to reflect the altered bone geometry.[18]

Gait Dynamics Simulations

The processing pipeline for analyzing both the baseline and deformed models (including five varus configurations) consisted of scaling, inverse kinematics, inverse dynamics, static optimization, and joint reaction force analysis. All procedures were implemented in OpenSim 4.2, and simulation results were time-normalized to 100% of the gait cycle.

During the scaling step, both segment lengths and mass properties (mass and inertia tensor) were adjusted using a measurement-based scaling method. This approach determines scale factors for each body segment by comparing distances between predefined model markers and their corresponding experimental marker locations. The 2392 musculoskeletal model contains predefined markers, and the Plug-in-Gait marker set employed in the gait analysis is compatible with this model.

Inverse kinematics was used to estimate joint angles from experimental walking data, without accounting for the forces or moments that drive the motion. A scaled subject-specific model and experimental gait data were used. At each time step of the recorded motion, the optimal joint angles that best reproduced the experimental kinematics

were computed. These angles were determined by solving a weighted least-squares optimization problem that minimized marker error, defined as the distance between experimental markers and their corresponding model markers.[16]

Net joint moments were calculated using the inverse dynamics method. This procedure incorporated the model's joint angles, angular velocities, and angular accelerations, along with experimental ground reaction forces and moments, to estimate the net joint moments. The equations of motion were solved iteratively based on the kinematic description and mass properties of the musculoskeletal model. Net reaction forces and moments at each joint were obtained by enforcing dynamic equilibrium and applying appropriate boundary conditions, including fixed supports, prescribed motions, and external loads.[19]

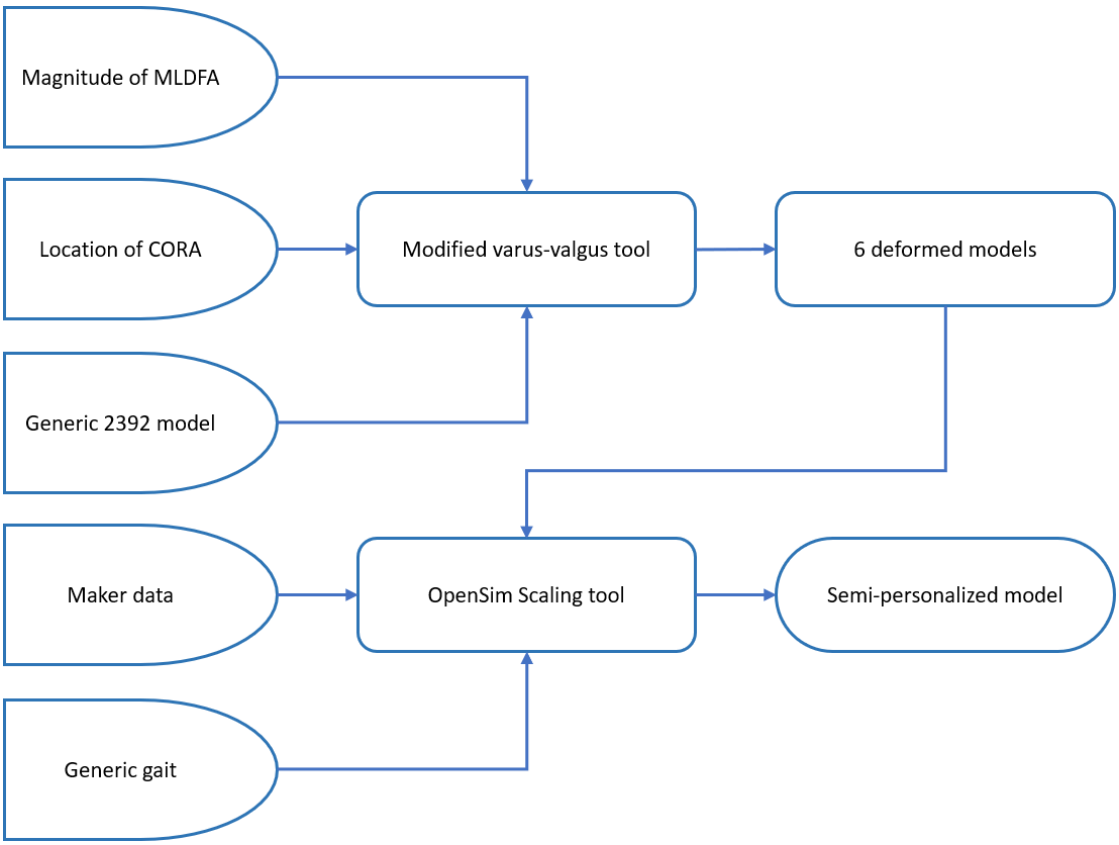

Figure 1. A flowchart for the steps involved in creating a semi-personalized model for a patient with femoral varus deformity

Joint reaction forces (JRFs) were computed using the Analyze tool in OpenSim through joint reaction analysis.[20] These forces were used to satisfy joint constraints, represent internal loading, and account for the combined effect of all external and muscle forces acting on the model. However, due to errors in motion data and limitations of the musculoskeletal model, the calculated JRFs occasionally violated Newton's second law.[21] To address this issue, residual forces and moments were applied to the pelvis segment of the model to ensure compliance with Newton's second law of motion.

Muscle moment arms were also calculated using the Analyze tool in OpenSim. Average moment arms were computed for both agonist and antagonist muscle groups, with grouping based on the mean moment arm in each anatomical plane across the gait cycle. Muscle moment arms were then classified into six categories for hip rotations (adductor/abductor, extensor/flexor, and internal/external rotator), two categories for ankle function (plantarflexor/dorsiflexor), and two categories for knee function (flexor/extensor).

The next stage involved applying the static optimization method to estimate muscle activations that reproduced the observed segment positions, velocities, accelerations, and external forces (e.g., ground reaction forces). Calculations were performed independently at each time frame, without integrating the equations of motion across time steps.

We categorized the muscle data into functional groups based on their anatomical roles during the gait cycle, and applied this classification to both muscle activation and muscle moment arm analysis. The hip flexors, which include the iliopsoas, rectus femoris, sartorius, and tensor fasciae latae, are responsible for hip flexion. The hip extensors comprised the gluteus maximus, semitendinosus, semimembranosus, biceps femoris (long

head), and both heads of the adductor magnus, which extend the hip. The hip abductors—gluteus medius, gluteus minimus, and tensor fasciae latae—facilitate movement of the leg away from the midline, whereas the hip adductors—pectineus, adductor longus, gracilis, adductor brevis, and both heads of the adductor magnus—bring the leg toward the midline. The hip internal rotators (tensor fasciae latae and gluteus minimus) rotate the hip inward. In contrast, the external rotators (gluteus maximus, sartorius, piriformis, gemellus superior, obturator internus, obturator externus, and quadratus femoris) perform the opposite action. At the knee, the flexors consist of the semimembranosus, semitendinosus, biceps femoris (both heads), gracilis, sartorius, gastrocnemius, plantaris, and popliteus, which enable knee flexion. The extensors included the rectus femoris, vastus lateralis, vastus medialis, and vastus intermedius, which extend the knee.

As recommended in previous studies, joint moments were normalized to body mass, enabling more accurate comparisons across individuals of different sizes. Specifically, joint moments were divided by the participant's body mass and expressed as Newton-meters per kilogram (N·m/kg). Joint contact forces were normalized to body weight to account for inter-individual variation in gravitational load. To compute the net load on each joint, we calculated the vector sum of forces across the sagittal, frontal, and transverse planes by summing the squares of the respective force components. This approach captures the combined multidirectional loading and provides a comprehensive measure of joint loading.[22] Muscle activations were normalized to the peak activation. Statistical analysis was performed using one-way ANOVAs with Tukey's post-hoc tests ($p < 0.05$) for both mean muscle activations and moment arms. Additionally, linear regression analyses were conducted for these variables across all CORA locations ($p < 0.05$), and results were presented graphically.

Validation

To validate our model, we used experimental data from a 36-year-old male subject presenting with knee pain. Radiographic assessment showed an MMPTA of 90° and an MLDFA of 89° for the right leg, and an MMPTA of 84° and an MLDFA of 91° for the left leg (extracted from X-ray images).[23,24] A semi-personalized model was created based on the subject's bony abnormalities and corresponding CORAs. Both generic and semi-personalized models were analyzed. The models were scaled and processed using the same inverse kinematics setup, with equal weighting applied to markers and coordinates. The mean errors of lower extremity markers during inverse kinematics were then calculated for both models.[25]

Results

During the gait cycle, joint angles and moments were analyzed for different varus deformity alignment models and compared with the generic model. The results indicated that certain dynamic variables were influenced by varus severity, whereas others remained unaffected [Figures 2 and 3]. Hip and knee flexion/extension angles were essentially unchanged. In contrast, the hip abduction/adduction angle increased significantly as the CORA was positioned closer to the hip joint. Hip rotation demonstrated a phase-dependent pattern, with greater proximal CORA positioning resulting in increased rotation during early stance, decreased rotation in late stance, and increased rotation again during the swing phase. At the ankle, plantar-/dorsiflexion decreased slightly, whereas the subtalar angle increased with CORA placement closer to the knee joint. Pelvic kinematics were also affected: pelvic rotation (twisting around the vertical axis) decreased moderately, while pelvic list (lateral pelvic displacement) increased considerably with more proximal CORA positioning. Pelvic tilt (anterior–posterior pelvic rotation) increased during early stance, late stance, and swing, but decreased during mid-stance as the CORA moved proximally [Figure 2].

From a kinetics perspective [Figure 3], slight changes were observed in pelvic tilt, hip flexion/extension, and knee flexion/extension moments during the swing phase. At the same time, these variables remained largely unaffected in stance. With more proximal CORA positioning, pelvic rotational moments decreased in early stance and late stance/swing, and pelvic list moments decreased moderately. In contrast, hip rotational moments increased—slightly during stance and more substantially during swing. Hip abduction/adduction moments, however, were moderately reduced as the CORA was positioned closer to the hip joint. At the ankle, plantar-/dorsiflexion and subtalar moments were largely unaffected during swing, but both exhibited alterations during stance, with the subtalar moment showing considerable changes.

Resultant hip, knee, and ankle joint reaction forces (JRFs) were obtained for the different models [Figure 4]. CORA positioning had a pronounced effect on hip JRF, particularly at the first and second peaks of the stance phase. Proximal CORA placement reduced hip JRF, while producing a moderate increase in ankle contact force. In contrast, knee JRF was largely unaffected, showing only slight increases during the first peak of stance and during swing as the CORA moved closer to the hip joint.

The average muscle activations and their standard deviations for each functional muscle group were analyzed across the gait cycle [Figure 5]. The gait cycle was divided into stance and swing phases, each exhibiting distinct patterns of muscle activity. Muscle activations were normalized by dividing each value by the maximum activation recorded across all muscles and trials, identified during the stance phase. This normalization enabled meaningful comparisons between muscle groups and facilitated the interpretation of their relative contributions to movement. Linear regression analysis revealed that muscle group activations either decreased (hip abduction, hip extension, hip internal rotation, and knee extension), increased (hip external rotation, ankle dorsiflexion, and ankle plantarflexion), or remained relatively unchanged (knee flexion, hip flexion, and hip adduction) with more proximal CORA positioning. The effect of CORA positioning was strongest for hip abduction, hip extension, hip internal/external rotation, and ankle dorsiflexion ($R > 0.9$), and weakest for hip flexion, hip adduction, and ankle plantarflexion ($R < 0.5$). Finally, statistical testing (one-way ANOVA with Tukey's post-hoc analysis) confirmed that

differences between the deformed models and the baseline condition were significant ($p < 0.001$).

Average moment arms of agonist and antagonist muscle groups during the gait cycle were calculated and are presented in [Figure 6]. To better illustrate differences between values, moment arms were visualized on a logarithmic scale. Linear regression analysis showed that average moment arms decreased for hip flexion/extension, hip external rotation, and ankle dorsiflexion, but increased for hip internal rotation, hip adduction, hip abduction, ankle plantarflexion, and knee flexion with more proximal CORA positioning. The influence of CORA positioning was pronounced for nearly all reported moment arms ($R > 0.9$), except knee extension ($R < 0.5$). Finally, differences between the deformed models and the baseline condition were statistically significant ($p < 0.001$, one-way ANOVA with Tukey's post-hoc analysis).

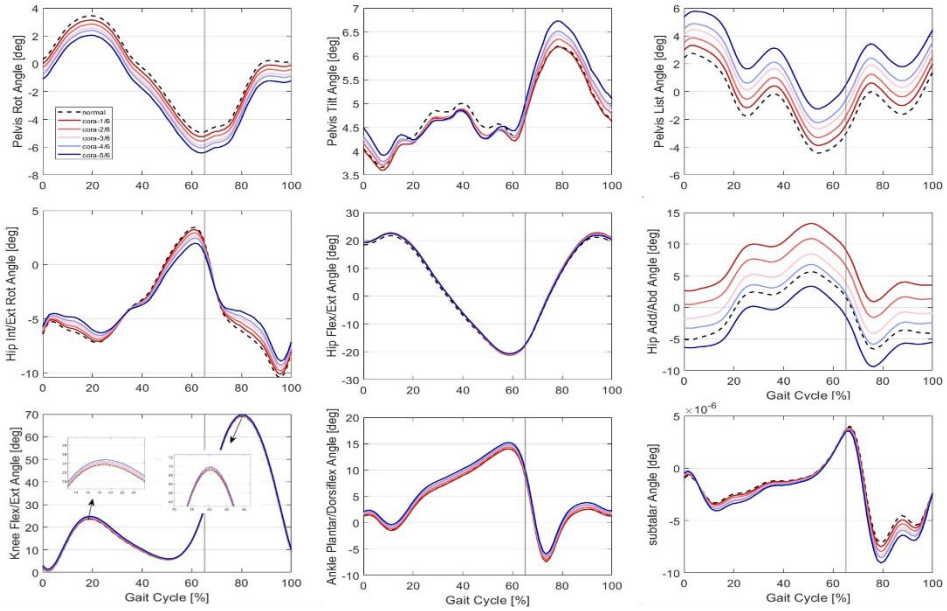

Figure 2. Joint kinematic. The obtained waveforms from all deformed and normal models are shown in solid curves and dashed curves respectively. Gray vertical lines indicate the end of the stance phase

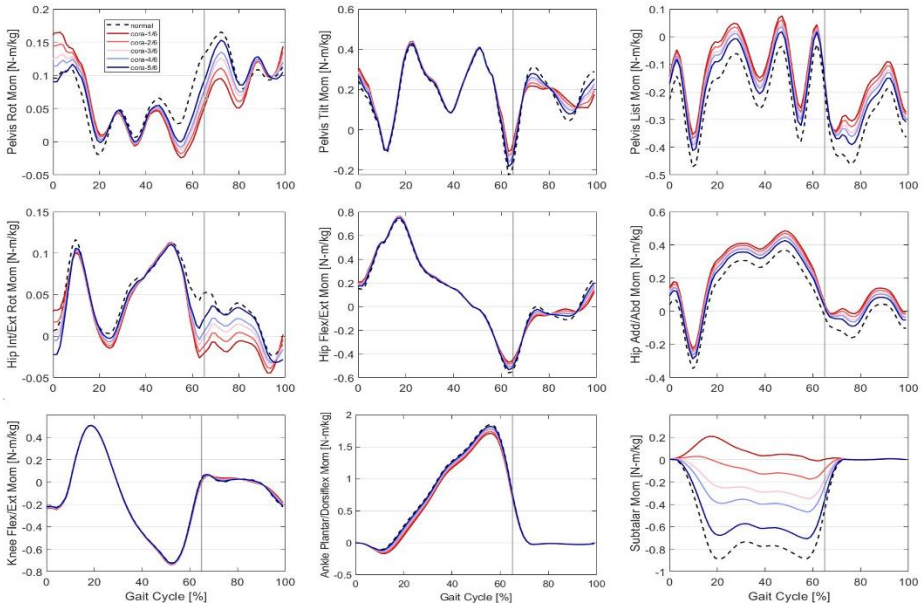

Figure 3. Joint kinetics. The obtained waveforms from all deformed and normal models are shown in solid curves and dashed curves respectively. Gray vertical lines indicate the end of the stance phase

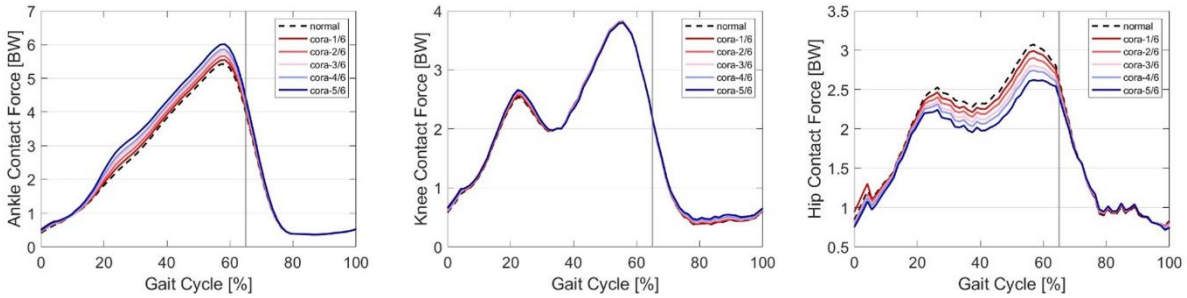

Figure 4. Resultant ankle, knee and hip JRFs obtained for all deformed (solid curves) and normal (dashed curves) models during the gait cycle described by BW (body wight). Gray vertical lines indicate the end of the stance phase

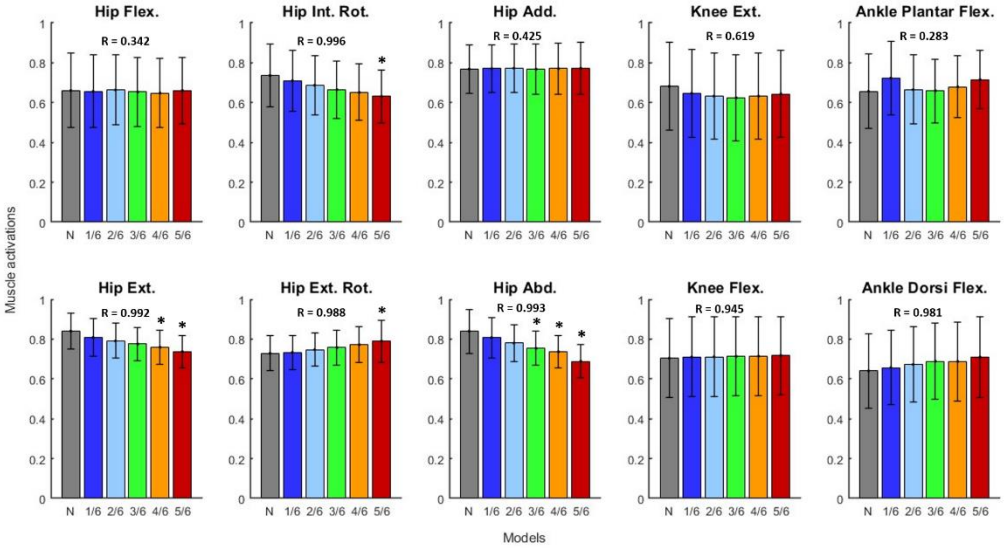

Figure 5. Bar plots showing the mean ± standard deviation muscle activations during the gait cycle. The values are indicated for all deformed models with different CORA location (colored bars) and normal model (gray bar)

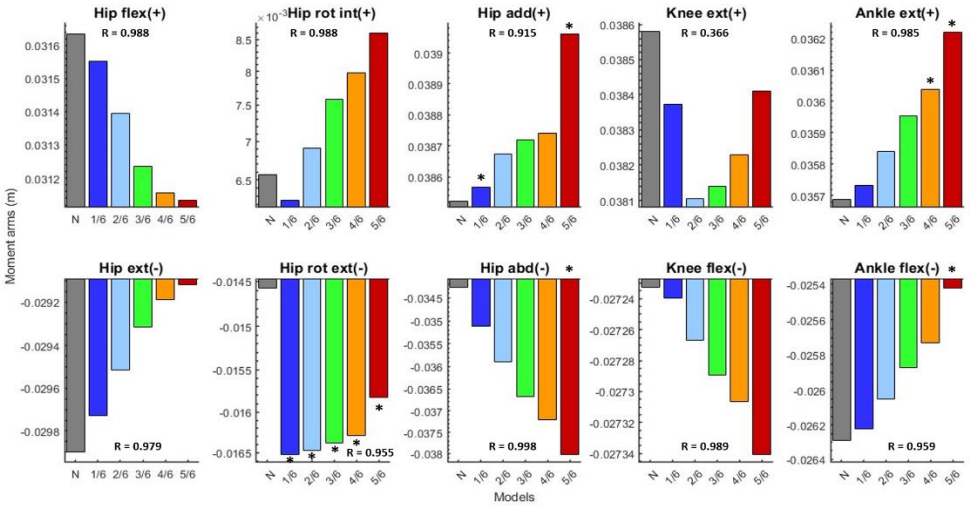

Figure 6. Average moment arm during the gait cycle obtained from agonist and antagonist muscle groups. Moment arms of agonist and antagonist are visualized in bar plots with positive or negative values, respectively. The values are indicated for all deformed models with different CORA location (colored bars) and normal model (gray bar). Negative values indicate that the direction of the muscle's force vector acts in an opposing direction relative to the joint movement

Discussion

This study introduced a method to improve varus deformity modeling by explicitly incorporating the precise location of the CORA. We evaluated the effect of CORA positioning on lower-limb biomechanics in femoral varus deformity using musculoskeletal modeling and numerical simulations. The analysis assessed how variation in the origin of the deformity influences joint kinetics and kinematics. Inverse kinematics, inverse dynamics, and static optimization were employed to compute joint angles, net joint moments, muscle activations, joint reaction forces, and muscle moment arms. The primary focus was on comparing simulations across different levels of femoral varus deformity rather than on subject-specific joint load predictions. Finally, the approach was validated with experimental data. The semi-personalized model substantially reduced marker error in inverse kinematic analysis, highlighting the effectiveness of the proposed method for individuals with femoral varus deformity.

The primary contribution of this work is the assessment of how variations in femoral varus origin influence joint kinematics. We found that changes in CORA positioning significantly affected pelvic and hip kinematics as well as pelvic, hip, and subtalar kinetics. Specifically, pelvic list, pelvic tilt, ankle plantar-/dorsiflexion, and knee flexion/extension angles increased as the CORA was positioned more proximally on the femur. Rotational alterations in the femur due to varus deformity were compensated mainly by hip abduction/adduction and pelvic list, reflecting the knee's limited degrees of freedom in abduction/adduction [Figure 2]. In contrast, subtalar, hip abduction/adduction, and pelvic internal/external rotational angles decreased with more proximal CORA positioning. Hip internal/external rotation increased during early stance and swing, but decreased in late stance, when the CORA was located closer to the hip joint.

From a kinetic perspective, as the CORA shifts proximally toward the hip joint, pelvic list, hip adduction/abduction, and subtalar moments decrease in magnitude; however, all deformity models still demonstrate higher values compared to baseline. Pelvic internal/external rotation, ankle plantar-/dorsiflexion, and hip internal/external rotation exhibit lower peak values with more distal CORA locations; nevertheless, these values remain below baseline, particularly during late stance. Proximal CORA positioning results in increased ankle contact force and reduced hip contact force, as the longer knee moment arm associated with a proximal CORA alters the load distribution. Knee contact forces show only minor variations, which can be attributed to the one-degree-of-freedom (1DOF) definition of the knee joint. Most muscle activation patterns are largely unaffected; however, reductions are observed in hip abduction, hip extension, hip internal rotation, and knee extension, while increases occur in hip external rotation and ankle plantar flexion for varus deformities with a proximal CORA. Muscle moment arms generally show minimal significant changes. Specifically, hip abductor moment arms increase with proximal CORA, hip extensor moment arms decrease, hip internal rotators demonstrate larger moment arms, and hip external rotators decrease when the CORA is located close to the hip joint.

The credibility of our results is supported by three factors: (i) the use of a previously validated musculoskeletal model, (ii) the implementation of an open-source varus–valgus tool,[14,16] and (iii) comparisons with earlier studies reporting joint kinetics and kinematics in adolescents with varus deformity.[9,26] The overall trends observed in the inverse kinematics (joint angles) and inverse dynamics (joint moments) of patients with varus deformity compared with normally aligned lower limbs were consistent with these previous findings. For methodological validation, paired landmark errors during inverse kinematics were calculated for a patient with a 6° femoral varus deformity using both a generic and a semi-personalized model. The boxplots of these landmark errors are presented in [Figure 7]. Error magnitudes were consistently reduced across all landmarks when employing the semi-personalized model compared with the generic model. Consequently, subsequent analyses—such as inverse dynamics and muscle optimization—are also expected to benefit from this reduction. Our findings demonstrate the effectiveness of the proposed approach and align with recent reports. Tabeiy et al.[14] similarly showed that a semi-personalized method significantly decreases marker errors in inverse kinematics for patients with tibial varus deformity.

In musculoskeletal analysis, the use of generic models with a normal mechanical lateral distal femoral angle (MLDFA) of 90° may result in imprecise outcomes and potential clinical misinterpretation when evaluating patients with varus deformity.[23,27] This limitation arises because the origin of varus deformity is difficult to model and investigate without a definition based on the center of rotation of angulation (CORA). To address this issue, patient-specific models have been developed; however, these approaches are often time-consuming and costly. [13,28,29] As an alternative, we modified the varus–valgus tool to incorporate varus deformity into generic models using CORA positioning, thereby enabling more accurate representation of subjects with varus deformity.[14] The CORA location can be readily determined from patient geometry using either two-dimensional (2D) or three-dimensional (3D) imaging techniques.[30] Incorporating CORA into musculoskeletal modeling provides deeper insight into joint biomechanics (kinetics and kinematics) in three dimensions[31] and reveals the specific ways in which varus deformity can impair movement. Such information can support surgeons in designing more precise treatment strategies and in reducing the risk of adverse outcomes, including joint line obliquity, nonunion, and prolonged recovery.[32]

Acknowledging the limitations of the present study, future work will employ forward muscle-driven models, rather than the inverse kinematics and dynamics approaches used here, as forward simulations are expected to yield more precise estimations of joint kinematics and kinetics.[33] The influence of CORA positioning on the tibia will also be investigated, since varus deformity may originate from either the tibia or the femur, and accounting for tibial CORA will

provide a more comprehensive understanding of its biomechanical effects.[15] In addition, a more complex muscle-driven musculoskeletal model with greater joint degrees of freedom will be implemented, as the single degree-of-freedom assumption for the knee represents a notable simplification.[33,34] Finally, the results will be validated more rigorously using experimental data from patients with varus deformity.

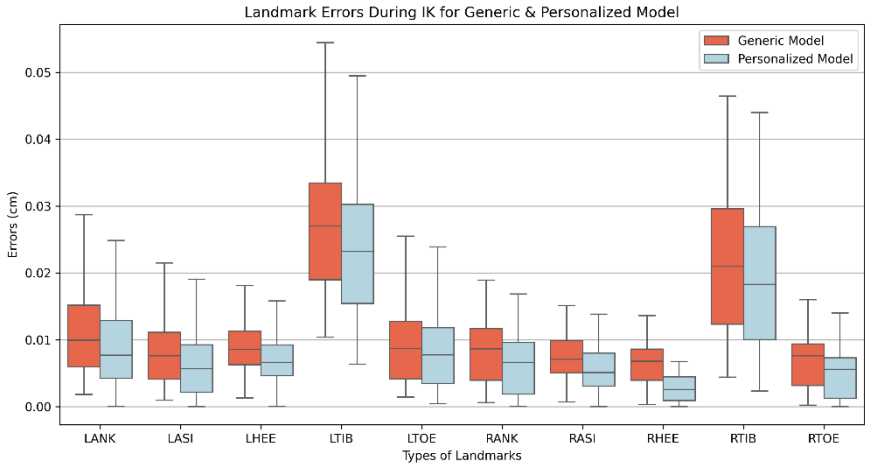

Figure 7. Boxplot to describe the distribution of the errors between experimental data and inverse kinematics for both generic model (red) and semi-personalized model (light blue). LANK/RANK: Left/Right ankle joint, LASI/RASI: Left/Right anterior superior iliac spine, LHEE/RHEE: Left/Right heel, LTIB/RTIB: Left/Right tibia, and LTOE/RTOE: Left/Right big toe are lower limb landmarks (markers)

Conclusion

This study presents a computational modeling approach that incorporates precise CORA positioning to improve the estimation of joint biomechanics. Simulations with varying CORA positions demonstrated that the origin of varus deformity primarily influences ankle, pelvic, and hip kinematics, as well as ankle, hip, and subtalar kinetics. The primary surgical objective is to restore normal loading conditions, and the use of semi-personalized models can enhance the accuracy of these estimations, thereby supporting preoperative planning. Nevertheless, more advanced modeling—such as subject-specific approaches with additional joint degrees of freedom—is required to validate the clinical implications of these findings.

Acknowledgement

N/A

Authors Contribution: Authors who conceived and designed the analysis: Reyhaneh Rostamian, Morad Karimpour, Masoud Shariat Panahi/Authors who collected the data: Morad Karimpour, Reyhaneh Rostamian/Authors who contributed data or analysis tools: Reyhaneh Rostamian, Mahdie Aghasizade, Morad Karimpour/Authors who performed the analysis: Reyhaneh Rostamian/Authors who wrote or revised the paper: Reyhaneh Rostamian, Morad Karimpour, Masoud Shariat Panahi, Mahdie Aghasizade, Hadi G. Kashani

Declaration of Conflict of Interest: The author(s) do NOT have any potential conflicts of interest for this manuscript.

Declaration of Funding: The author(s) received NO financial support for the preparation, research, authorship, and publication of this manuscript.

Declaration of Ethical Approval for Study: All procedures performed in studies involving human participants were conducted according to the ethical standards of the institutional research committee and with the 1964 Helsinki Declaration and its later amendments. The protocol of this study was approved by the Ethical Committee of the University of Tehran (Reference: ETHIC-202403-1180).

Declaration of Informed Consent: There is no information (names, initials, hospital identification numbers, or photographs) in the submitted manuscript that can be used to identify patients.

Reyhaneh Rostamian PhD [1]
Masoud Shariat Panahi PhD [1]
Morad Karimpour PhD [1]
Mahdie Aghasizade PhD [1]
Hadi G. Kashani PhD [1]

1 School of Mechanical Engineering, University of Tehran, Tehran, Iran

References

1. Paley D, Herzenberg JE, Tetsworth K, McKie J, Bhave A. Deformity Planning for Frontal and Sagittal Plane Corrective Osteotomies. Orthop Clin North Am. 1994;25(3):425-465. doi:10.1016/S0030-5898(20)31927-1.
2. Heller MO, Taylor WR, Perka C, Duda GN. The influence of alignment on the musculoskeletal loading conditions at the knee. Langenbeck's Arch Surg. 2003;388(5):291-297. doi:10.1007/s00423-003-0406-2.
3. Khani Y, Bisadi A, Salmani A, et al. Can Artificial Intelligence Reliably and Accurately Measure Lower Limb Alignment: A Systematic Review and Meta-Analysis. Arch Bone Jt Surg. 2025;13(7):383-394. doi:10.22038/abjs.2025.84846.3864.
4. Shah K, Solan M, Dawe E. The gait cycle and its variations with disease and injury. Orthop Trauma. 2020;34(3):153-160. doi:10.1016/j.mporth.2020.03.009.
5. Deshpande BR, Katz JN, Solomon DH, et al. Number of Persons With Symptomatic Knee Osteoarthritis in the US: Impact of Race and Ethnicity, Age, Sex, and Obesity. Arthritis Care Res (Hoboken). 2016;68(12):1743-1750. doi:10.1002/ACR.22897.
6. Shima H, Walter H, Gholamreza R. Alteration of Lower Limb Kinematics and Kinetics due to Bilateral Triple Arthrodesis. Arch Bone Jt Surg. 2023;11:711-716. doi:10.22038/abjs.2023.68704.3246.
7. Dehcheshmeh FG, Nourbakhsh MR, Farsani ZA, Bazrgari B, Arab AM. Kinematic Analysis of Pelvic and Lower Limb Joints during Stand-to-sit Movement in Individuals with Chronic Low Back Pain: A cross-sectional study. Arch Bone Jt Surg. 2024;12(8):587-596. doi:10.22038/ABJS.2024.76840.3551.
8. Sherafat Vaziri A, Ahmadzadeh H, Hosseinzadeh N. How to Perform an Accurate and Safe Medial Open Wedge High Tibial Osteotomy; A Technical Note. Arch Bone Jt Surg. 2025;13(6):378-382. doi:10.22038/abjs.2025.81222.3703.
9. Whatling GM, Biggs PR, Elson DW, Metcalfe A, Wilson C, Holt C. High tibial osteotomy results in improved frontal plane knee moments, gait patterns and patient-reported outcomes. Knee Surgery, Sport Traumatol Arthrosc. 2020;28(9):2872-2882. doi:10.1007/s00167-019-05644-7.
10. Sherafatvaziri A, Salkhori O, Razi M, et al. Practice Trends in Primary Total Knee Arthroplasty among Members of the Iranian Society of Knee Surgery, Arthroscopy, and Sports Traumatology. Arch Bone Jt Surg. 2025;13(6):359-366. doi:10.22038/ABJS.2025.85348.3889.
11. Caldwell LK, Laubach LL, Barrios JA. Effect of specific gait modifications on medial knee loading, metabolic cost and perception of task difficulty. Clin Biomech. 2013;28(6):649-654. doi:10.1016/j.clinbiomech.2013.05.012.
12. Killen BA, Brito da Luz S, Lloyd DG, et al. Automated creation and tuning of personalised muscle paths for OpenSim musculoskeletal models of the knee joint. Biomech Model Mechanobiol. 2021;20(2):521-533. doi:10.1007/S10237-020-01398-1.
13. Smale KB, Conconi M, Sancisi N, et al. Effect of implementing magnetic resonance imaging for patient-specific OpenSim models on lower-body kinematics and knee ligament lengths. J Biomech. 2019;83:9-15. doi:10.1016/J.JBIOMECH.2018.11.016.
14. Tabeiy S, Karimpour M, Shirvani A, Vaziri AS. The Influence of Knee Varus Deformity on the Kinematic and Dynamic Characteristics of Musculoskeletal Models During Gait. Comput Methods Biomech Biomed Engin. 2025 Apr 9:1-8. doi: 10.1080/10255842.2025.2487817.
15. Paley D. Principles of Deformity Correction. 3rd ed. (Herzenberg m JE, ed.). Springer-Verlag Berlin Heidelberg New York; 2005.
16. Delp SL, Anderson FC, Arnold AS, et al. OpenSim: open-source software to create and analyze dynamic simulations of movement. IEEE Trans Biomed Eng. 2007;54(11):1940-1950. doi:10.1109/TBME.2007.901024.
17. Delp SL, Loan JP, Hoy MG, Zajac FE, Topp EL, Rosen JM. An Interactive Graphics-Based Model of the Lower Extremity to Study Orthopaedic Surgical Procedures. IEEE Trans Biomed Eng. 1990;37(8):757-767. doi:10.1109/10.102791.
18. Rostamian R, Shariat-Panahi M, Karimpour M, Kashani HG. Compensatory gait deviations during single-limb stance in patients with excessive tibial torsion. In2023 30th National and 8th International Iranian Conference on Biomedical Engineering (ICBME) 2023 (pp. 244-248). IEEE.
19. Hicks J. Tutorial 3 - Scaling, Inverse Kinematics, and Inverse Dynamics. Availabla at: https://opensimconfluence.atlassian.net/wiki/spaces/OpenSim/pages/53089741/Tutorial+3+-+Scaling+Inverse+Kinematics+and+Inverse+Dynamics. Accessed May 11, 2024.
20. Kainz H, Mindler GT, Kranzl A. Influence of femoral anteversion angle and neck-shaft angle on muscle forces and joint loading during walking. PLoS One. 2023;18(10):e0291458. doi: 10.1371/journal.pone.0291458.
21. OpenSim - Event Details. Avaailable at: https://simtk.org/projects/jointreaction. Accessed May 11, 2024.
22. Falisse A, Van Rossom S, Gijsbers J, et al. OpenSim versus human body model: a comparison study for the lower limbs during gait. J Appl Biomech. 2018;34(6):496-502. doi: 10.1123/jab.2017-0156.
23. Rostamian R, Panahi MS, Karimpour M, Nokiani AA. Automatic assessment of lower limb deformities using high - resolution X - ray images. BMC Musculoskelet Disord. 2025;26(1):521. doi:10.1186/s12891-025-08784-9.
24. SimTK. Knee Varus/Valgus Malalignment Tool for OpenSim Models. Available at: https://simtk.org/projects/var-val-tool. Accessed April 25, 2025.
25. Davis J. johnjdavisiv/opensim-ik-errors: Calculate errors for each marker when doing inverse kinematics in OpenSim. Available at: https://github.com/johnjdavisiv/opensim-ik-errors. Accessed April 25, 2025.
26. De Pieri E, Nüesch C, Pagenstert G, Viehweger E, Egloff C, Mündermann A. High tibial osteotomy effectively redistributes compressive knee loads during walking. J Orthop Res. 2023;41(3):591-600. doi: 10.1002/jor.25403.
27. Latifpoor M, Sarzaeem MM, Amoozadeh Omrani F, Raissi Dehkordi S. Comparison of Functional Outcomes of Two Knee Arthroplasty Techniques (Total Knee Arthroplasty and Unicompartmental Knee Arthroplasty) for the Treatment of

Osteoarthritis, simultaneously done in the Same Patients. Arch Bone Jt Surg. 2024;12(10):695-700. doi:10.22038/abjs.2024.75050.3469.

28. Modenese L, Montefiori E, Wang A, Wesarg S, Viceconti M, Mazzà C. Investigation of the dependence of joint contact forces on musculotendon parameters using a codified workflow for image-based modelling. J Biomech. 2018;73:108-118. doi:10.1016/J.JBIOMECH.2018.03.039.
29. Valente G, Crimi G, Vanella N, Schileo E, Taddei F. nmsBuilder: Freeware to create subject-specific musculoskeletal models for OpenSim. Comput Methods Programs Biomed. 2017;152:85-92. doi:10.1016/J.CMPB.2017.09.012.
30. Rostamian R, Shariat Panahi M, Karimpour M, Kashani HG, Abi A. A deep learning-based multi-view approach to automatic 3D landmarking and deformity assessment of lower limb. Sci Rep. 2025;15(1):1-12. doi:10.1038/s41598-024-84387-z.
31. Ahrend MD, Baumgartner H, Ihle C, Histing T, Schröter S, Finger F. Influence of axial limb rotation on radiographic lower limb alignment: a systematic review. Arch Orthop Trauma Surg. 2022;142(11):3349-3366. doi:10.1007/S00402-021-04163-W/FIGURES/4.
32. Di Y, Wu G, Zhang G, Guo X, Li L. Observation on Curative Effect of Minimally Invasive Osteotomy Combined with Ilizarov Technique in the Treatment of Knee Osteoarthritis with Varus Deformity. Bone Arthrosurgery Sci. 2023;1(2):7-14. doi:10.26689/BAS.V1I2.5250.
33. Wheatley BB, Chaclas NA, Seeley MA. Patellofemoral Joint Load and Knee Abduction/Adduction Moment are Sensitive to Variations in Femoral Version and Individual Muscle Forces. J Orthop Res. 2023;41(3):570-582. doi:10.1002/jor.25396.
34. Besier TF, Pal S, Draper CE, et al. The Role of Cartilage Stress in Patellofemoral Pain. Med Sci Sports Exerc. 2015;47(11):2416. doi:10.1249/MSS.0000000000000685.